LDH and TiO_2/LDH-type nanocomposite systems : a systematic study on structural characteristics

Reference:

Seftel Elena, Niarchos M., Vordos N., Nolan J. W., Mertens M., Mitropoulos A. Ch., Vansant Etienne, Cool Pegie.- LDH and TiO_2/LDH-type nanocomposite systems : a systematic study on structural characteristics

Microporous and mesoporous materials: zeolites, clays, carbons and related materials - ISSN 1387-1811 - 203(2015), p. 208-215

DOI: http://dx.doi.org/doi:10.1016/j.micromeso.2014.10.029

LDH and TiO_2/LDH-type nanocomposite systems: a systematic study on structural characteristics

E. M. Seftel[1*], M. Niarchos[2], N. Vordos[2], J. W. Nolan[2], M. Mertens[3], A. Ch. Mitropoulos[2], E. F. Vansant[1, 2], P. Cool[1]

(1) Laboratory of Adsorption and Catalysis, Department of Chemistry, University of Antwerpen (CDE), Universiteitsplein 1, 2610 Wilrijk, Antwerpen, Belgium

(2) Eastern Macedonia and Thrace Institute of Technology, Kavala 65404, Greece

(3) VITO Flemish Institute for Technological Research, Boeretang 200, B-2400, Belgium

* Corresponding author: elena.seftel@uantwerpen.be or seftel_elena@yahoo.com

Abstract: The work reported involves a detailed characterization study on a series of nanocomposite systems comprising layered double hydroxides and TiO_2 seeds with anatase crystal structure. The TiO_2/LDH nanocomposite structural and textural features were varied by the isomorphous substitution within the LDH sheets network of the divalent cations (Zn^{2+} by Cu^{2+}) and the trivalent cations (Al^{3+} by Fe^{3+} or Ti^{4+}) respectively. In depth characterization was obtained by using a combination of XRD, N_2 sorption, SEM, TEM/EDX and SAXS characterization techniques in order to maximize the structural information of the parent and modified LDH materials. An increase material compactness on the TiO_2/LDH nanocomposites was observed due to the accommodation of the TiO_2 seeds within the mesopores together with a surface coating. SAXS observations indicated the modification of the morphology of the parent LDH samples by the addition of the TiO_2 seeds suggesting the rearrangement of the LDH layers during the nanocomposite formation.

Keywords: Titania, Layered Double Hydroxides, Nanocomposites, brucite-like sheets alteration, structural characterization

Introduction

Fabrication of nano-sized titania (TiO_2) with anatase crystal structure is nowadays a very attractive research topic due to its remarkable physicochemical properties as well as its potential applications in photocatalytic processes for the removal of environmentally dangerous pollutants from air [1, 2] and water streams [3-5], in solar energy conversion processes or hydrogen production [6].

However, the use of pure TiO_2 and moreover, the use at large scale, suffers from several drawbacks such as high recombination rates of the photo-generated electrons and holes, possibility to activate the material only under ultraviolet irradiation with wavelength between 300 and 400 nm, agglomeration to larger particles reducing its photocatalytic performances or difficulty in separation after the end of the processes [5]. Therefore, an interesting research pathway is the development of new TiO_2-based photocatalysts with tailored properties.

The current research in the preparation of nanocomposite materials containing TiO_2 reports the use of different inorganic matrices, such as silica-based mesoporous materials [7, 8], zeolites [9-11] or cationic clays [12-14] and more recently anionic clays (type Layered Double Hydroxides) [3, 5, 15]. We have previously studied the possibility to support titania nanoseeds with anatase crystal structure on the MgAl-LDH material as representative for this class of layered clays. The nanocomposites proved to behave as superior photocatalysts when compared with the commercial TiO_2 P25 powder. Moreover, the use of such nanocomposite material showed also advantages in the separation step, for instance the

TiO_2/LDH nanocomposite was able to separate by natural sedimentation within minutes, while the commercial P25 could not separate for several days [5].

More recently, we observed that the immobilization of the titania on the LDH-type matrices may bring additional important advantages, namely the formation of new active sites which can participate in the photocatalytic process. The LDH configuration provides a good dispersion of the cations within the sheets which can act as charge separation centers as well as initiators of different types of heterojunctions enhancing the photocatalytic efficiency [15].

Layered double hydroxides are a class of naturally occurring clays, also called hydrotalcites or anionic clays. Their structure arises from the substitution of divalent cations with trivalent cations within the brucite structure ($Mg(OH)_2$) giving rise to a positive charge on these sheets. This positive charge is electro-balanced by anionic species which are located together with the water molecules in the interlayer gallery [16, 17].

These materials are described by the general formula $[M^{II}_{1-x}M^{III}_x(OH)_2]^{x+}\ A^{n-}_{x/n} \bullet mH_2O$, in which the divalent M^{II} and trivalent M^{III} cations may be Mg^{2+}, Zn^{2+}, Ni^{2+}, Cu^{2+}, Al^{3+}, Fe^{3+}, Ti^{4+}, Sn^{4+}, etc, and the A^{n-} can be almost any organic or inorganic anion [16].

Layered double hydroxides are currently synthesized by various techniques, such as co-precipitation at constant pH, sol-gel, urea hydrolysis, etc. Among them the co-precipitation technique seems to be the best method to produce LDHs since it allows the use of homogeneous precursor solutions.

Nowadays, these materials are currently used in a wide variety of applications due to their interesting and unique properties, such as anionic exchange, tunable porosity, memory

effect, basic character due to the highly hydroxylated surfaces, good dispersion of the cations within the layered sheets, easy to manipulate or to insert catalytic active sites by modulating either the brucite-like sheets composition or the nature of the anionic species within the interlayer gallery.

Various characterization techniques (X-ray Diffraction (XRD), N_2 sorption, Scanning Electron Microscopy (SEM), Transmission Electron Microscopy with Energy Dispersive X – ray System (TEM/EDX) and Small Angle X-ray Scattering (SAXS)) were used to investigate the structural properties of different LDHs and TiO_2 modified LDH materials. Correlation of the results from different characterization techniques were made to maximize the structural information of parent and modified LDH materials.

The aim of this work is to prepare different types of LDH and TiO_2/LDH nanocomposite systems by modulating the layered sheet composition. The influence on the structural characteristics as well as the morphology and porosity tuning due to the replacement of the divalent (Zn^{2+} by Cu^{2+}) or trivalent (Al^{3+} by Fe^{3+} and Ti^{4+}) cations on the properties of the resulting nanocomposites is investigated in-depth.

Experimental Section

Besides the parent LDH materials, a series of TiO_2/LDH nanocomposite samples were prepared by the deposition of anatase seeds on layered matrices with different sheets composition using a three-step procedure we previously described elsewhere [5].

LDHs synthesis

Layered double hydroxides containing different cationic species in the brucite-like sheets (like Zn^{2+}, Cu^{2+}, Al^{3+}, Fe^{3+} or Ti^{4+}) were obtained by the co-precipitation method at constant

pH. The synthesis was realized by mixing appropriate amounts of metal salt solutions (1M in total) and co-precipitation by the slowly addition of a mixture of 1M $NaOH/Na_2CO_3$ solution at a fixed pH value depending on the cationic species. The resultant slurries were aged at 353K under magnetic stirring for 18 h, separated by centrifugation, washed several times with water and dried at 353K overnight.

Anatase seeds synthesis

TiO_2 anatase seeds were prepared by the controlled hydrolysis of an ethanolic solution of titanium (IV) tetra-isopropoxide as previously described elsewhere [18, 19]. After the hydrothermal synthesis step at 353K for 4 h of the white suspension, the anatase seeds were recuperated by centrifugation, washed with distilled water, air-dried in ambient conditions and calcined at 673K.

Formation of the TiO_2/LDH nanocomposites

The TiO_2/LDH nanocomposites were obtained by suspending appropriate amounts of anatase seeds in distilled water followed by the addition of 1g of the as-prepared LDH support. The obtained suspensions were vigorously stirred for 48h at room temperature, separated by centrifugation at the end of the reaction, washed with distilled water and air-dried at room temperature.

The details on the sample notation and pH used for the synthesis of the LDH-type matrices are given in Table 1.

Table 1.

Characterization techniques

XRD measurements

The structure and the crystal phases of the as synthesized solids were investigated by X-ray diffraction (XRD) recorded on a PANalytical X'Pert PRO MPD diffractometer with filtered CuKα radiation; measurements were done in the 2θ mode using a bracket sample holder with a scanning speed of 0.04°/4 s in continuous mode.

Chemical Analysis

The chemical analysis of the parent LDH materials and TiO_2 content in the final modified nanocomposites was investigated by Electron Probe Microanalysis (EPMA) technique carried out on a JEOLJXA-733 apparatus.

Table 2.

Porosity and Surface area

Porosity and surface area studies were performed on a Quantachrome Quadrasorb-SI automated gas adsorption system using nitrogen as the absorbate at liquid nitrogen temperature (77K). All the samples were outgassed under vacuum for 16 h at 298K before the adsorption measurements. The surface area was calculated using the BET method in the range of relative pressure 0.05–0.35. The pore size distributions were deduced from the adsorption branches of the isotherms using the Barrett–Joyner–Halenda (BJH) method. The total pore volumes were calculated from the amount of N_2 vapor adsorbed at a relative pressure of 0.95.

SEM analysis

The particle morphology was investigated by a FEI QUANTA FEG 250 field emission scanning electron microscope (SEM).

TEM/EDX Analysis

TEM analysis was performed using a JEOL JEM 2100 microscope operated at 200kV and equipped with an Oxford Instruments X-Max 80T EDX and a Gatan Orius SC1000 CCD Camera.

SAXS measurements

The porous structures of the various LDH samples were examined by means of Small Angle X-ray Scattering (SAXS). The SAXS experiments were carried out at 298K by a JJ-Xray SAXS equipped with a 2D Rigaku detector using X-ray radiation with a wavelength of 1.54 Å (CuKα). The sample chamber was under vacuum and all the analyses were done after correction of cosmic radiation , empty beam, tape and direct beam for the same time. The distance between the samples and the detector was 0.8 m.

Results and Discussions

The XRD patterns before and after the TiO_2 deposition, towards the formation of the nanocomposites, are shown in Figure 1. The XRD patterns correspond well with the typical layered structure showing the high intense basal reflections at low 2 theta angles and the lower intensity non-basal reflections at higher 2 theta angles [17].

Figure 1.

The reflections of *hkl* planes (003) and (110) are typical for the LDH structures, and the intensities reflect the degree of crystallization and eventual distortions of the octahedral

brucite-like sheets. Copper-containing layered double hydroxides represent a particular type of composition in the family of the LDH compounds, due to the presence of the Jahn-Teller effect which leads to the distortion of the octahedral units around the Cu sites [20-22]. This effect appears in the CuZnAl-LDH systems (Figure 1B) and becomes more evident in the CuZnFeTi-LDH systems (Figure 1C) when the lowered intensity of the basal reflection corresponding to the (003) plane is observed, which can be correlated to the presence of the Cu^{2+} cations within the brucite-like sheets leading to the distortion of the octahedral units.

Table 3.

The *c* unit cell parameter value of about 2.3 nm, obtained for the as-synthesized materials, corresponds well with values previously reported for the carbonate-containing LDHs [16, 17]. The detailed analysis of the *c* value indicated that this unit cell parameter decreases slightly with the insertion of the Cu^{2+} cations within the brucite-like sheets which may be assigned to the differences in the electrostatic interactions between the interlayer anionic species and the cationic sheets, taking into consideration that only 0.2 moles of Zn^{2+} cations (3 moles in total) were substituted with Cu^{2+} cations in the brucite-like sheets. Going further and substituting the trivalent cations and also part of these with tetravalent Ti^{4+} cations leads to the decrease of the *c* value up to 2.07 nm due to the creation of extra positive charges on the layered sheets. At the same time, the *a* unit cell parameter increases gradually from the ZnAl-LDH material to the multicomponent CuZnFeTi-LDH material. This observation may be assigned to the differences in the cationic radii and also to the different M-O bond length in the octahedral units. Therefore, we may conclude based on the variations of the *a* and *c* unit cell parameters values that the Cu^{2+}, Fe^{3+} and Ti^{4+} were successfully incorporated within the brucite-like sheets of the obtained LDH materials.

The chemical composition analysis realized by Electron Probe Microanalysis (EPMA) measurements indicates that up to 30wt% of TiO_2 nanoparticles of approximately 6 - 8 nm (Table 3) are embedded into the layered matrices.

After the incorporation of the TiO_2 seeds within the nanocomposites, characteristic diffraction peaks for both LDH and anatase phases may be clearly distinguished in the XRD patterns (Figure 1 A, B and C, b patterns). During the deposition process when mixing the suspension of the TiO_2 nanoparticles with the LDH matrices, the immobilization of the TiO_2 onto the highly hydroxylated layers of LDHs via interface affinity leads to a more disordered nanocomposite structure, therefore weakening of the (003) reflection in the diffraction patterns, like observed for the TiO_2/ZnAl-LDH and TiO_2/CuZnAl-LDH samples. Moreover, for the TiO_2/CuZnAl-LDH sample, the reflection characteristic for the (003) plane is slightly shifted to lower 2θ angle. This observation may be correlated with the change if the structural ordering during the TiO_2 deposition stage. Several researchers focused previously on the CuAl-LDH systems [23, 24] and described that during a prolonged hydrothermal treatment at moderate temperatures, a rearrangement of the stacking faults occurs. The *a* unit cell parameter maintain the same value as before the TiO_2 incorporation indicating that no changes in the sheets structural characteristics occurred during the formation of the nanocomposites. Therefore, the shift of the (003) reflection in the XRD pattern of the TiO_2/CuZnAl-LDH nanocomposite is related with the change in the symmetry of the carbonate anions within the interlayer gallery. It is reported that the Cu-Al systems are exception among LDHs in that ordering is observed during hydrothermal treatments [24]. In the present experimental conditions, the deposition step of the TiO_2 seeds on the CuZnAl-LDH matrix during two days of vigorous stirring at room temperature could lead to a

different orientation of the carbonate anions within the interlayer gallery and therefore, a shift in the position of the (003) reflection as observed in Figure 1B.

The surface area S_{BET} values were estimated from the N_2 sorption measurements at 77K (Table 3). The adsorption/desorption isotherms together with the pore size distributions for the TiO_2/LDH nanocomposites are presented in Figure 2 in comparison with the parent LDH matrices.

Figure 2.

Generally, the LDH-type materials are characterized by an external surface mesoporosity since the N_2 diameter is larger than the interlamellar space for carbonate-containing LDHs, so that the pore volume measured corresponds to the interparticle pores [25, 26]. As previously reported, changes in the porosity characteristics may be attributed to the alteration of the microscopic morphology due to the presence of different cations within the structure [27].

The shape of all isotherms of the LDH matrices, before TiO_2 deposition, is Type IV according to the IUPAC classification typical for mesoporous materials. On the other hand, differences in the hysteresis loops indicate different types of pore shapes which can be correlated with the different composition of the layered sheets. The ZnAl-LDH material shows a Type IV isotherm with a small plateau at high relative pressures and a H_1 hysteresis loop which is usually explained by the presence of agglomerates defined as rigidly joined particles [28]. Upon substitution of part of Zn^{2+} cations with Cu^{2+} cations within the LDH lattice, a major decrease of porosity is observed probably due to the distortion of the octahedral units lowering the mesoporosity characteristics of the obtained material. The desorption is delayed up to lower relative pressures, changing the shape of the hysteresis loop into H_4 and

the formation of very small slit-shaped pores as also indicated by the pore size distribution (Figure 2B, inset picture). The insertion of the tetravalent Ti^{4+} cations within the LDH matrix leads to a major increase of the mesoporous surface area with the concomitant change of the isotherm into Type II with the H_3 hysteresis loop attributed to aggregates of plate-like particles containing slit-shaped pores [27].

After the TiO_2 incorporation, the hysteresis in the isotherms indicate that the nanocomposites are mesoporous with the diameter of the pores in the theoretical range of 2 – 50 nm. The pore size distribution was calculated from the adsorption branch of each isotherm using the BJH method (Table 1) [28]. For the TiO_2/LDH nanocomposite systems, the maximum of the distribution curve is shifted towards smaller pore sizes indicating the insertion of the TiO_2 nanoparticles within the clay mesopores. The calculated pore diameters are into the range of 4.8 – 5.4 nm. It can be noticed that the TiO_2/CuZnAl-LDH nanocomposite increases after the TiO_2 seeds deposition. This may be attributed to the rearrangement of the stacking faults, therefore change in the structural ordering of the CuZnAl-LDH sheets during the TiO_2 deposition stage which can be well correlated with the XRD observations.

Scanning Electron Microscopy (SEM) was used to investigate in detail the microstructure of the LDH and TiO_2/LDH nanocomposite systems. Representative SEM micrographs are presented in Figure 3. Typical morphology showing interconnected plate-like particles is observed for the ZnAl-LDH matrix (Figure 3a). The observed morphology can be correlated with the XRD observations demonstrating that the material is well crystallized having the characteristic LDH-type structural and morphology features. When the TiO_2 seeds are embedded into the LDH matrix towards the formation of the TiO_2/ZnAl-LDH nanocomposite

system, the LDH plates are organized around the TiO_2 seeds leading to the formation of spherical-shaped rigidly joined nanoparticles (Figure 3b) reducing also the porosity features as also observed from the N_2-sorption measurements (Table 3).

The SEM micrograph recorded for the CuZnAl-LDH material shows the formation of smaller plate-like particles with a higher agglomeration degree, which can be associated with the formation of brucite-like sheets with distorted octahedral units around the Cu sites. The preservation of the plate-like morphology after the copper substitution into the brucite-like sheets clearly supports the supposition of the formation of a typical layered material and can be well correlated with the XRD observations. When the TiO_2 seeds are embedded into the CuZnAl-LDH matrix, the SEM images indicates also a higher degree of agglomeration of the nanoparticles as compared with the parent CuZnAl-LDH matrix (Figure 3d).

Figure 3.

When the tetravalent Ti^{4+} cations are accommodated within the brucite-like sheets, the SEM images indicate the formation of a material characterized by an interconnected plate-like morphology but major decrease in the particle size can be detected (Figure 3e), which was previously reported for the Ti-containing LDH materials [27]. This behavior may be well correlated with the major increase of the specific surface area observed for the CuZnFeTi-LDH sample (Table 3). After the TiO_2 incorporation and the formation of the TiO_2/CuZnFeTi-LDH nanocomposite, the obtained SEM image indicates again the preservation of the plate-like morphology of the LDH component contributing to the high specific surface area recorded for this sample.

Figure 4.

Structural information on the LDH and TiO_2 modified nanocomposites were further obtained by using the Transmission Electron Microscopy (TEM). Representative TEM images of the parent ZnAl-LDH (Figure 4A) show that the material displays the typical plate-like morphology which is changed after the TiO_2 seeds incorporation towards the nanocomposite system (Figure 4B).

The fractal structure of the various LDH samples and TiO_2 seeds were studied with Small Angle X-ray Scattering (SAXS) technique. In general SAXS curves usually can be divided into three basic regions (Guinier, Fractal and Porod) as shown in Figure 5.

Figure 5.

The scatter vector from Guinier to fractal region defined as q_G and from fractal to porod as q_p. The mean size of the clustes ξ can be defined by $2\pi/ q_{G.}$ From q_p the size of the elementary particles α is $2\pi/ q_{p.}$ When from a ln–ln plot of I(q)/q versus q can be made and the slope of the line -α (attenuation index, if $1<\alpha<3$), D_m is equal to α. From the same plot, if $3<\alpha<4$ the surface fractal dimension D_s equals 6-a. SAXS investigations on this type of nanocomposites are very limited [29, 30]. In general, three characteristics can be observed: the mean size of the clusters (ξ), which can be connected to the form of the network, the mean size of the primary particles (α), which form the cluster, and the fractal dimension (D with Ds and Dm represented respectively mass distribution and surface coarseness/structure compactness). All the SAXS curves of the various LDH samples (without and with TiO_2 modification) and the TiO_2 seeds are shown in Figure 6. As shown by Fei He et al. [31], the parameters ξ , α and D (Ds and Dm) were calculated for all the parent and TiO_2 modified LDH samples (Table 4). In general all SAXS curves have similar slopes in the same regions (Fractal

and Porod regions). The TiO_2 material has fractal characteristics due to a well structure[30]. This means that the fractal parameters are comparable.

However, for the CuZnAl – LDH the radius of gyration (R_g) shows more important differences compared to the other samples, meaning that the average of square center of means distances is lower in CuZnAl – LDH compared to the others which refer to the differences in S_{BET}.

The morphology of the parent LDH samples modifies with the addition of TiO_2 suggesting a rearrangement of the LDH layers forming a higher mesoporosity, indicating changes in pore size distribution and TEM images.

The observed increase in the material compactness of the modified LDH samples could be the results of the presence of titania in the interparticle spaces (mesopores) together with a surface coating. This is in agreement with the observations of E. M. Seftel at. all [5].

Table 4.

Figure 6.

Conclusions

A series of nanocomposite systems were prepared by a simple synthesis route which involves the deposition of anatase TiO_2 seeds onto LDH matrices. The structure of the obtained nanocomposites was varied by changing the brucite-like sheets composition. It was found that the nature of the isomorphously substituted cations has a direct influence on the structural as well as on the textural features of the obtained TiO_2/LDH nanocomposites. The presence of the Cu^{2+} cations leads to a distortion of the octahedral sheets around the Cu sites as observed using the XRD technique. This has a direct influence on the microtexture of

the obtained nanocomposite on which a higher degree of agglomeration was observed. On the other hand, by substituting the trivalent Al^{3+} cations with Fe^{3+} and furthermore with tetravalent Ti^{4+} cations, the obtained materials are characterized by the same interconnected plate-like morphology but major decrease in the particle size was detected. Detailed investigation by TEM and SAXS techniques indicated an increased compactness on the TiO_2/LDH nanocomposites due to the accommodation of the TiO_2 seeds within the mesopores together with a surface coating.

ACKNOWLEDGEMENTS

E. M. Seftel greatly acknowledges the Fund for Scientific Research – Flanders (FWO – Vlaanderen) for financial support. This work was also supported by the Nanocapillary Project (*Thales Framework*) of the Eastern Macedonia & Thrace Institute of Technology (Ministry of Education and Religious Affairs, Culture and Sports, NSRF 2007–2013).

References

[1] R. de_Richter, S. Caillol, Journal of Photochemistry and Photobiology C: Photochemistry Reviews 12 (2011) 1-19.
[2] Y. Paz, Applied Catalysis B: Environmental 99 (2010) 448-460.
[3] G. Carja, A. Nakajima, S. Dranca, C. Dranca, K. Okada, The Journal of Physical Chemistry C 114 (2010) 14722-14728.
[4] J.C. K. Bubacz, D. Dolat, A. W. Morawski, Polish Journal of Environmental Studies 19 (2010) 685-691.
[5] E.M. Seftel, E. Popovici, E. Beyers, M. Mertens, H.Y. Zhu, E.F. Vansant, P. Cool, J Nanosci Nanotechnol 10 (2010) 8227-8233.
[6] G.I.N. Waterhouse, A.K. Wahab, M. Al-Oufi, V. Jovic, D.H. Anjum, D. Sun-Waterhouse, J. Llorca, H. Idriss, Sci. Rep. 3 (2013).
[7] J. Ida, T. Yoshikawa, T. Matsuyama, H. Yamamoto, Advanced Powder Technology 18 (2007) 329-348.
[8] K. Inumaru, M. Yasui, T. Kasahara, K. Yamaguchi, A. Yasuda, S. Yamanaka, Journal of Materials Chemistry 21 (2011) 12117-12125.
[9] T. Kamegawa, R. Kido, D. Yamahana, H. Yamashita, Microporous and Mesoporous Materials 165 (2013) 142-147.
[10] L. You-ji, C. Wei, Catalysis Science & Technology 1 (2011) 802-809.
[11] L.-P. Wu, X.-J. Li, Z.-H. Yuan, Y. Chen, Catalysis Communications 11 (2009) 67-70.

[12] K.-I. Shimizu, T. Kaneko, T. Fujishima, T. Kodama, H. Yoshida, Y. Kitayama, Applied Catalysis A: General 225 (2002) 185-191.
[13] S. Ouidri, C. Guillard, V. Caps, H. Khalaf, Applied Clay Science 48 (2010) 431-437.
[14] H.Y. Zhu, J.A. Orthman, J.Y. Li, J.C. Zhao, G.J. Churchman, E.F. Vansant, Chemistry of Materials 14 (2002) 5037-5044.
[15] E.M. Seftel, M. Mertens, P. Cool, Applied Catalysis B: Environmental 134–135 (2013) 274-285.
[16] F. Cavani, F. Trifirò, A. Vaccari, Catalysis Today 11 (1991) 173-301.
[17] Z.P.X. P. S. Braterman, F. Yarberry Handbook of Layered Materials, Marcel Dekker Inc, , New York, 2004.
[18] I. Kartini, D. Menzies, D. Blake, J.C.D. da Costa, P. Meredith, J.D. Riches, G.Q. Lu, Journal of Materials Chemistry 14 (2004) 2917-2921.
[19] G. Bertoni, E. Beyers, J. Verbeeck, M. Mertens, P. Cool, E.F. Vansant, G. Van Tendeloo, Ultramicroscopy 106 (2006) 630-635.
[20] G. Carja, R. Nakamura, H. Niiyama, Applied Catalysis A: General 236 (2002) 91-102.
[21] M. Crivello, C. Pérez, J. Fernández, G. Eimer, E. Herrero, S. Casuscelli, E. Rodríguez-Castellón, Applied Catalysis A: General 317 (2007) 11-19.
[22] N. Ahmed, Y. Shibata, T. Taniguchi, Y. Izumi, Journal of Catalysis 279 (2011) 123-135.
[23] C. Busetto, G. Del Piero, G. Manara, F. Trifirò, A. Vaccari, Journal of Catalysis 85 (1984) 260-266.
[24] S. Britto, P. Vishnu Kamath, Journal of Solid State Chemistry 182 (2009) 1193-1199.
[25] P. Benito, F.M. Labajos, J. Rocha, V. Rives, Microporous and Mesoporous Materials 94 (2006) 148-158.
[26] G. Carja, R. Nakamura, T. Aida, H. Niiyama, Microporous and Mesoporous Materials 47 (2001) 275-284.
[27] E.M. Seftel, E. Popovici, M. Mertens, G. Van Tendeloo, P. Cool, E.F. Vansant, Microporous and Mesoporous Materials 111 (2008) 12-17.
[28] F. Rouquerol, J. Rouquerol, K. Sing, in: F. Rouquerol, J. Rouquerol, K. Sing (Eds.), Adsorption by Powders and Porous Solids, Academic Press, London, 1999, pp. 191-217.
[29] J. Mrowiec-Białoń, L. Pająk, A.B. Jarzębski, A.I. Lachowski, J.J. Malinowski, Langmuir 13 (1997) 6310-6314.
[30] S.N.C. O.B. Pavlova-Verevkina, Y.A. Shechuk, L.A Ozerina, A.N. Ozerin, Material Science Poland 25 (2007) 825-834.
[31] X.H. Fei He, Mingwei Li and Sumei Zhang, Journal of Ceramic Processing Research 9 (2008) 389-392.

Table caption

Table 1. Sample identity and synthesis parameters.

Table 2. Initial and final chemical composition calculated based on the EPMA results.

Table 3. Structural characteristics and porosity data for the studied LDHs, TiO_2 and TiO_2/LDH nanocomposite materials.

Table 4. The fitting fractal parameters by SAXS analysis.

Table 1.

Parent LDH		**TiO_2/LDH nanocomposites**	
Sample	Co-precipitation pH	Sample	Deposition pH
ZnAl-LDH	7- 7.5	TiO_2/ZnAl-LDH	7
CuZnAl-LDH	7 – 7.5	TiO_2/CuZnAl-LDH	7
CuZnFeTi-LDH	10	TiO_2/CuZnFeTi-LDH	8 - 9

Table 2.

Parent LDH				
Sample	[a]Molar cationic ratio		[b]*X*	
	Initial	Final	Initial	Final
ZnAl-LDH	3 : 1	2.31 : 1	0.25	0.325
CuZnAl-LDH	0.2 : 2.8 : 1	0.213 : 2.98 : 0.99	0.25	0.238
CuZnFeTi-LDH	0.2 : 2.8 : 0.8 : 0.2	0.221 : 3.09 : 0.79 : 0.2	0.25	0.232
TiO_2/LDH nanocomposites				
Sample	[a]Molar cationic ratio (LDH phase)		[b]*X*	
	Initial	Final	Initial	Final
TiO_2/ZnAl-LDH	2.31 : 1	1.94 : 1	0.325	0.34
TiO_2/CuZnAl-LDH	0.213 : 2.98 : 0.99	0.142 : 1.988 : 0.98	0.238	0.32
TiO_2/CuZnFeTi-LDH	0.221 : 3.09 : 0.79 : 0.2	0.219 : 3.07 : 0.79 : 0.19	0.232	0.233

[a]Molar cationic ratio initially introduced in the synthesis mixture and finally in the as-synthesized materials, respectively; [b]$X = M^{III}/M^{II}+M^{III}+M^{IV}$

Table 3.

Sample	*c*, nm	*a*, nm	[a]D_{LDH}, nm	[a]D_{TiO2}, nm	S_{BET}, m^2/g	TV_p, cc/g	D_p, nm	[b]wt% TiO_2
ZnAl-LDH	2.33	0.307	8.77	-	25	0.145	22.6	-
TiO_2/ZnAl-LDH	2.39	0.307	4.93	6.6	21	0.054	5.4	27
CuZnAl-LDH	2.34	0.309	5.04	-	5	0.018	16.4	-
TiO_2/CuZnAl-LDH	2.65	0.309	4.55	8.1	36	0.087	4.8	23
CuZnFeTi-LDH	2.07	0.31	4.3	-	140	0.393	16.3	-
TiO_2/CuZnFeTi-LDH	2.08	0.31	4.1	6.2	133	0.340	4.8	24
TiO_2	-	-	-	7.5	86	0.116	3.6	100

$c = 3d_{003}$, $a = 2d_{110}$, [a] Crystallite sizes (LDH and TiO_2, respectively) calculated using the Scherrer equation, S_{BET} – specific surface area calculated using the BET method, TV_p – total pore volume measured at p/p_0 of 0.95, D_p – pore diameter calculated using the BJH method, [b] Calculated based on the EPMA results.

Table 4.

Sample	ξ nm	α nm	D_s	D_m	R_g (nm)
TiO_2 seeds	59.97	11.99	2.866	3.194	
ZnAl-LDH	35.70	10.49	2.580	3.420	19.9
TiO_2 /ZnAl-LDH	83.95	10.76	2.147	3.853	17.7
CuZnAl-LDH	59.96	15.55	2.000	3.999	15.8
TiO_2/CuZnAl-LDH	59.69	10.76	2.144	3.855	19.1
CuZnFeTi-LDH	59.97	19.98	2.38	3.62	20.5
TiO2/CuZnFeTi-LDH	59.97	15.55	2.04	3.96	21.8

*$\xi=2\pi/q_G$ (q_G is the scatter vector of the Guinier region), $a=2\pi/q_p$ (q_p is the scatter vector of the fractal region), D_s is the surface fractal and D_m is the mass fractal [31].

Figure caption

Figure 1. The XRD patterns of A: (a) ZnAl-LDH, (b) TiO_2/ZnAl-LDH, (c) TiO_2; B: (a) CuZnAl-LDH, (b) TiO_2/CuZnAl-LDH, (c) TiO_2 and C: (a) CuZnFeTi-LDH, (b) TiO_2/CuZnFeTi-LDH and (c) TiO_2 samples. * TiO_2 with anatase crystal structure.

Figure 2. N_2 adsorption/desorption isotherms at 77K and pore size distribution (inserted picture) of the A: ZnAl-LDH vs. TiO_2/ZnAl-LDH; B: CuZnAl-LDH vs. TiO_2/CuZnAl-LDH and C: CuZnFeTi-LDH vs. TiO_2/CuZnFeTi-LDH.

Figure 3. SEM micrographs of (a) ZnAl-LDH, (b) TiO_2/ZnAl-LDH, (c) CuZnAl-LDH, (d) TiO_2/CuZnAl-LDH, (e) CuZnFeTi-LDH and (f) TiO_2/CuZnFeTi-LDH samples.

Figure 4: Representative TEM images of A: ZnAl-LDH and B: TiO2/ZnAl-LDH and B, B': the corresponding Energy dispersive X-ray (EDX) analysis.

Figure 5. General SAXS pattern. The general SAXS curve, divided into three regions (Guimier, Fractal and Porod).

Figure 6. The SAXS results of A: (a) ZnAl-LDH, (b) TiO_2/ZnAl-LDH, (c) TiO_2; B: (a) CuZnAl-LDH, (b) TiO_2/ CuZnAl-LDH, (c) TiO_2 and C: (a) CuZnFeTi-LDH, (b) TiO_2/ CuZnFeTi-LDH and (c) TiO_2 samples.

Figure(s)

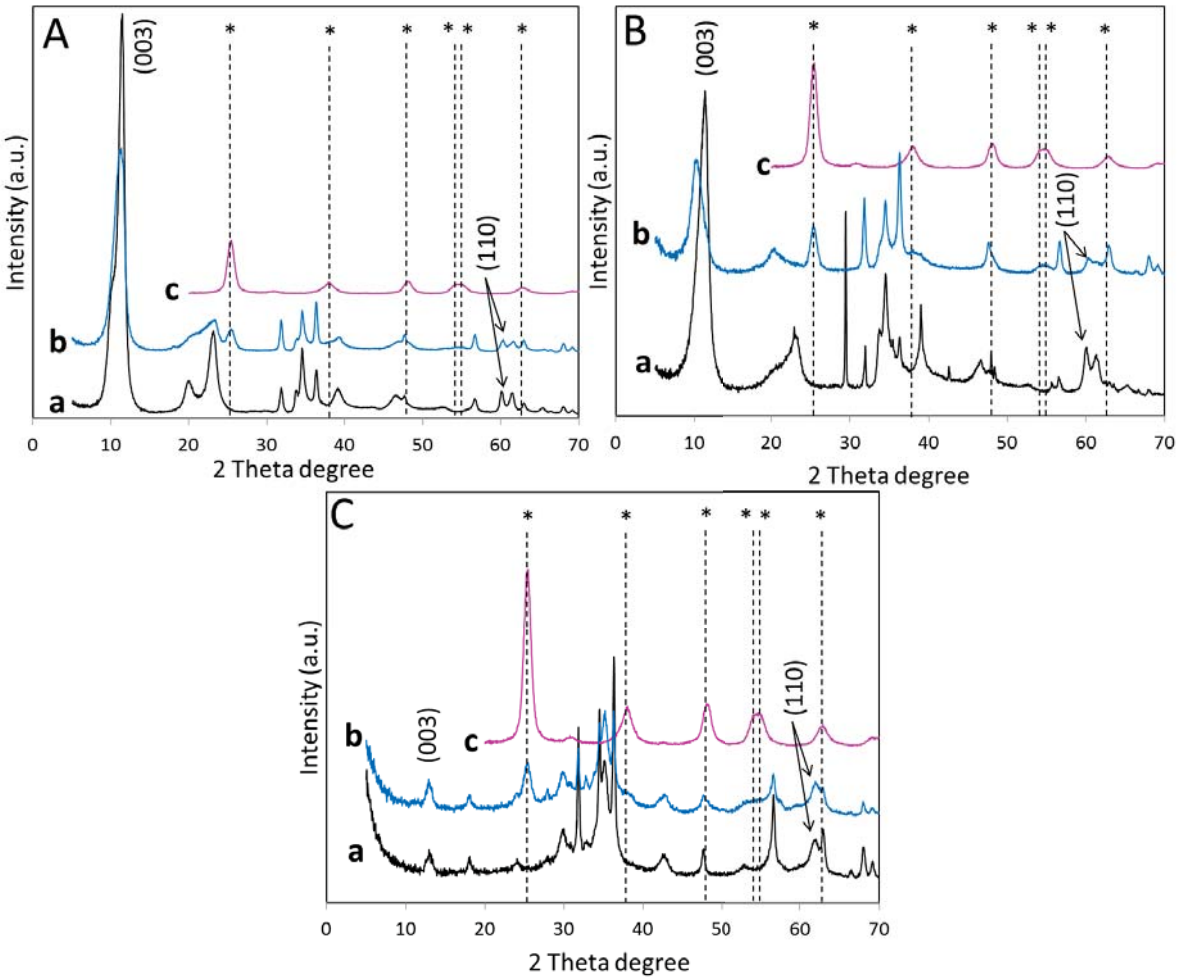

Figure 1.

Figure(s)

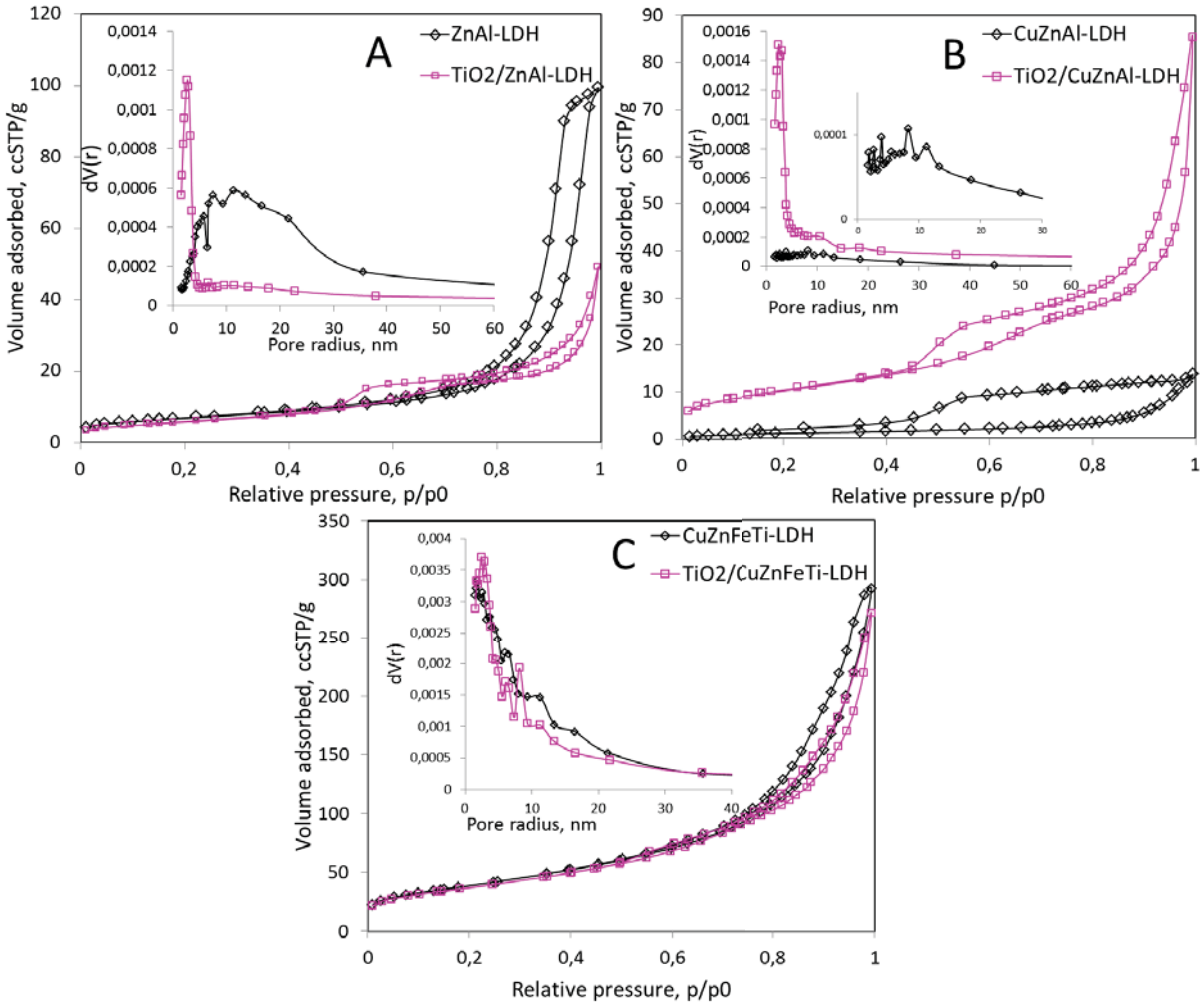

Figure 2.

Figure(s)

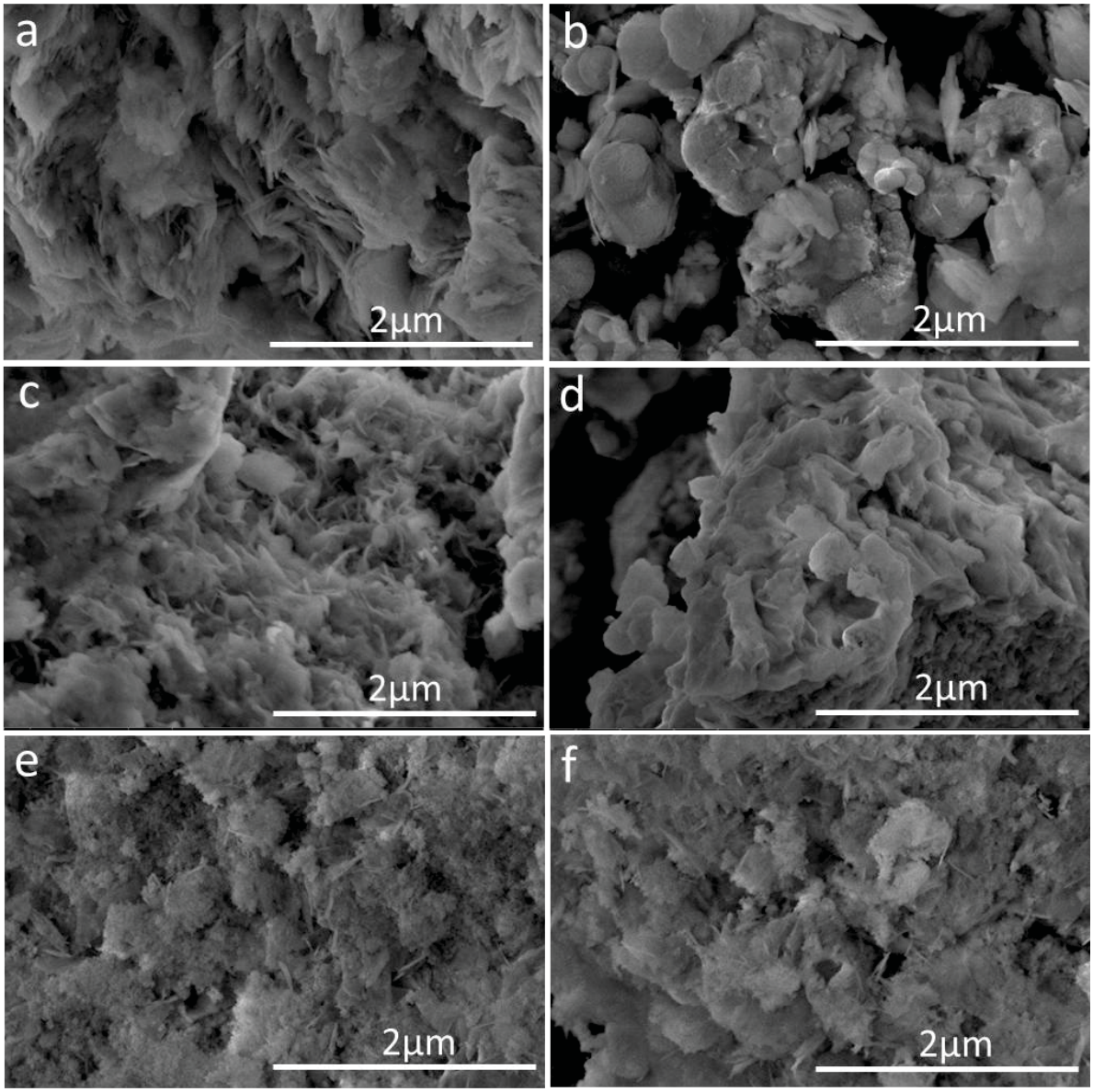

Figure 3.

Figure(s)

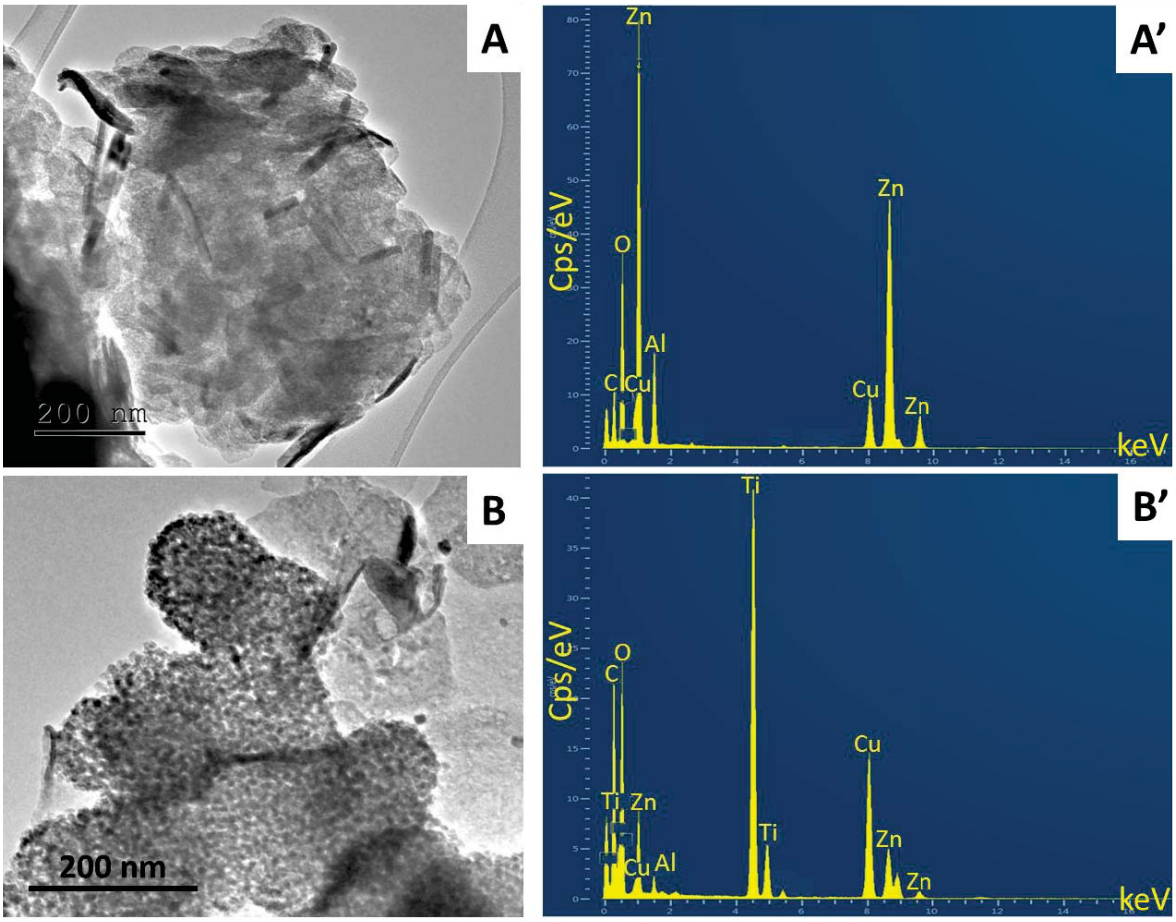

Figure 4.

Figure(s)

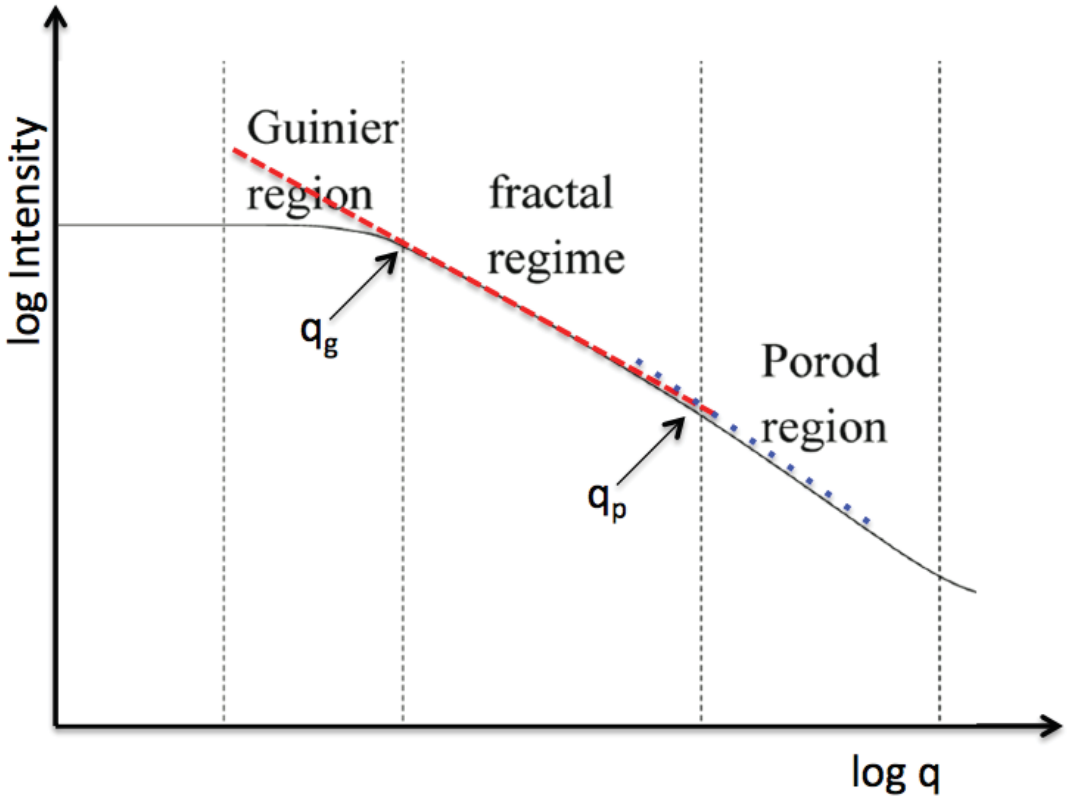

Figure 5.

Figure(s)

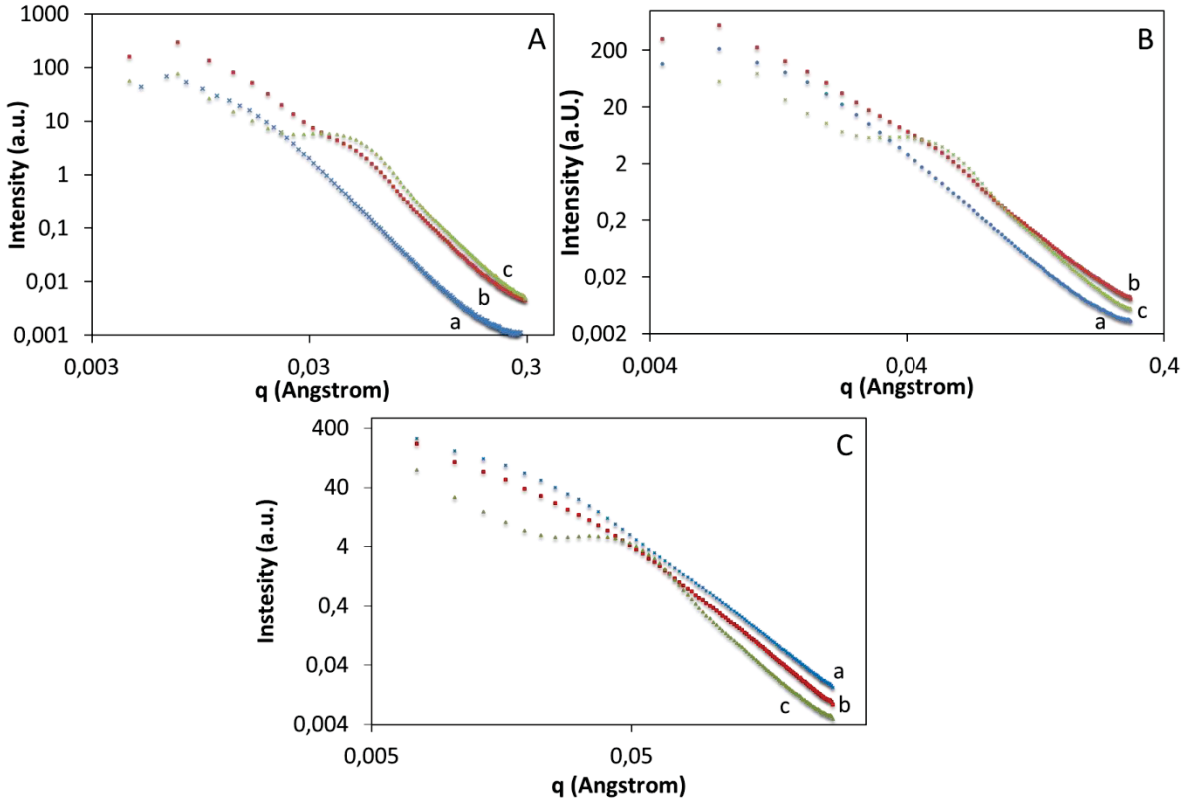

Figure 5.